E|DPC-2017

Electric Drives Production Conference and Exhibition

2017
7th International

Electric Drives Production Conference

5th and 6th December 2017
Wuerzburg, Germany

Program and Exhibition Brochure

Gold Supporter:

MARSILLI

Aluminium Supporter:

Bühler Motor

MAGCAM advanced magnet inspection

Exhibitors:

bdtronic

Breuckmann e-mobility

BROCKHAUS MEASUREMENTS

eta S.p.A.

DEMAK GROUP RESIN DISPENSING TECHNOLOGY

FVA Forschungsvereinigung Antriebstechnik e.V.

HÜBERS

imc

SMZ WICKEL- UND MONTAGETECHNIK AG

STIEFELMAYER lasertechnik

voestalpine ONE STEP AHEAD.

Wieland

AMA Verband für Sensorik + Messtechnik Innovationen verbinden

BÜHLER MOTOR MECHATRONIC AWARD 2017

Cluster Automotive

Cluster Leistungselektronik

FCPE

Technical Sponsor:

IEEE

Financal Sponsor:

FAPS

FAU FRIEDRICH-ALEXANDER UNIVERSITÄT ERLANGEN-NÜRNBERG

A conference held by:

SV Veranstaltungen

Static and Cyclic Mechanical Loads inside the Rotor Lamination of High-Speed PMSM

Jan Karthaus and Kay Hameyer
Institute of Electrical Machines (IEM)
RWTH Aachen University
Aachen, Germany
jan.karthaus@iem.rwth-aachen.de

***Abstract*—Rotors of high-speed electrical machines are subject to high static and cyclic mechanical loads which influence the operational machine behavior due to magnetic deviation. Therefore, it is essential to study the detailed mechanical stress distribution inside the rotor. This allows a better understanding of the electrical machine's behavior for high-speed applications. This knowledge can be used for a better electrical machine design. In this paper, a measurement approach is presented to study the mechanical stress distribution caused by mechanical static and cyclic loads inside a high-speed PMSM rotor. For analyzing the stress distribution, the rotor deformation is measured which leads to a deformation characteristic dependent on material and magnet arrangement. Furthermore, the deformation of cyclically loaded specimens is studied.**

Keywords—high-speed electrical machines; mechanical stress; machine design

I. Introduction

To increase drive performance and reduce installation space, electrical machines demand a high power density and thus high-speed rotors. The high-speed machines lead to new challenges in machine design and during its operation [1]: The speed-dependency of several loss components such as iron losses within the soft magnetic lamination, eddy current losses within the permanent magnets or bearing losses lead to an increase of heat produced inside the electrical machine. In addition, the dynamical behavior of the rotor for higher speeds causes additional vibrations which can be critical when in resonance. Furthermore, high speeds lead to an increase of mechanical stresses inside the rotor due to centrifugal forces. These stresses are superposed by local residual stresses injected due to the machine production (e.g. cutting process [2]).

Therefore, this paper focuses on the consequences of the high centrifugal forces inside the rotor when applying high speeds. Conventionally, the rotor geometry is simulated mechanically to determine the mechanical stress distribution inside the rotor. The simulation process requires boundary conditions and assumptions. The criteria of the highest allowed von-Mises stress is selected to find the most suitable rotor geometry [3]. A trade-off between width of the fillets around the magnet pockets and mechanical stress has to be performed to reduce magnetic leakage flux inside the rotor.

Such an approach does not consider any variations of magnetic properties inside the soft magnetic material caused by mechanical stress which is known as magneto-mechanical effect [4]. The magneto-mechanical effect describes variation in volume due to a magnetic field (magnetostriction) or the influence of mechanical stress on the magnetic properties (inverse magnetostriction), respectively. In electrical machines, this effect influences the magnetic flux path [5] or iron losses [6] which can cause a different operating behavior or overall machine's efficiency. These influences and consequences for the electrical machine's behavior have been studied in several scientific references but not in terms of improving the design process of electrical machines considering the magneto-mechanical effect [7, 8]. Models for the stress-dependency of the hysteresis curves or iron losses are in focus of current research [9–11].

Furthermore, rotors of high-speed traction drives are subject to a high varying cyclic load which initializes fatigue process inside the soft magnetic material [12]. This cyclic load leads to a deterioration of the magnetic properties before any mechanical deterioration becomes visible [13, 14].

Due to an increasing demand of electrical high-speed machines and the need of a better understanding of the influences of mechanical stress on the magnetic properties of the soft magnetic materials is required for well-designed electrical machine.

In this paper, the stress distribution of high-speed PMSM rotors is studied. Therefore, a test bench is set up which allows an in-situ measurement of the rotor deformation at high speed. In contrast to a mechanical simulation, this measurement permits a realistic conclusion about the mechanical stress distribution inside the rotor. Measurements with cyclically loaded specimens show the influence of cyclic stress on the rotor deformation.

II. Stress Distribution

A. Static Stress Distribution

The mechanical static stress distribution caused by centrifugal forces inside a rotating disc can be estimated by calculating the in-plane stress components (σ_r: radial

978-1-5386-1069-5/17/$31.00 ©2017 IEEE

component and σ_t: tangential component) of a disc with a concentric bore diameter:

$$\sigma_r(r) = (3+\nu)\frac{\rho\omega^2}{8}\left(r_1^2 + r_2^2 - \frac{r_1^2 r_2^2}{r^2} - r^2\right), \quad (1)$$

$$\sigma_t(r) = (3+\nu)\frac{\rho\omega^2}{8}\left(r_1^2 + r_2^2 - \frac{r_1^2 r_2^2}{r^2} - \frac{1+3\nu}{3+\nu}r^2\right). \quad (2)$$

ν is the Poisson's ratio, ρ the material density, ω the speed and r_1 or r_2, the inner or outer radius, respectively. Using the von-Mises criteria when shear stresses are neglected:

$$\sigma_{v,M} = \sqrt{\sigma_r^2 + \sigma_t^2 - \sigma_r\sigma_t}, \quad (3)$$

the stress distribution can be calculated.

In rotors of PMSM, the stress distribution is influenced by the geometry: The position and size of the magnet pockets affect the stress distribution as well as additional cut outs or the shaft-hub joint (notches or stress caused by shrink fitting).

In Fig. 1, the simulated von-Mises stress distribution inside the rotor lamination of a PMSM for different magnet arrangements at the maximum rotor speed of 12,000 min^{-1} is shown. The stress distribution is mainly influenced by the magnet arrangement: The lowest resulting stress is produced when using glued magnets inside the pockets; the highest stress results for unglued magnets. Due to the centrifugal forces, the unglued magnets are pushed against the outer pocket edge and cause a high load between pocket and rotor edge.

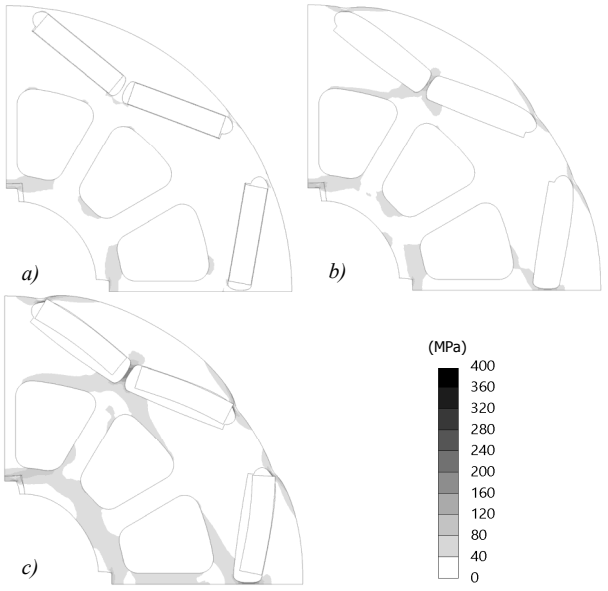

Fig. 1. Simulated von-Mises stress distribution of rotor at 12,000 min^{-1} for M350-50A: *a)* glued magnets, *b)* without magnets, *c)* unglued magnets (magnification scale: 1:170).

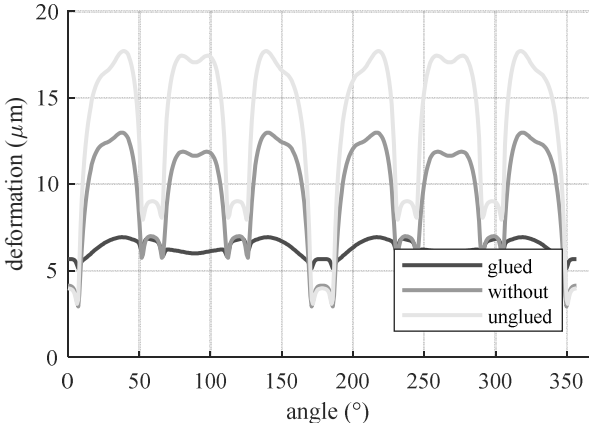

Fig. 2. Simulated corresponding rotor deformations for M350-50A at 12,000 min^{-1} for different magnet arrangements.

TABLE I. STEEL GRADES AND MECHANICAL PROPERTIES.

Steel grade	Density in kg/dm³	Yield strength in MPa	Young's Modulus in GPa
NO20	7.6	374	181
M270-35A	7.65	369	181
M350-50A	7.65	337	194

For the arrangement with glued magnets, the loads are distributed uniformly inside the rotor lamination. For each configuration, the maximum stress can be found at the notch at the inner radius. Other areas with high stress are the fillets between magnet pockets and outer rotor edge and between the pockets.

The different stress distribution causes a varying deformation contour on the rotor edge (Fig. 2). It can be observed that the deformation contour is not symmetric. This is caused by the notches at the inner rotor radius. For the arrangement with glued magnets, the deformation contour has a low amplitude whereas for the configuration with unglued magnets inside the pockets causes a high amplitude in deformation. Similar deformation contours can be observed for other steel grades such as NO20 or M270-35A. Differences occur due to the different yield strength and Young's Modulus (Tab. I).

B. Influence of Cyclic Stress

For several electrical machine applications such as traction drives for electric vehicles, the rotor is subject to a dynamically varying speed. In case of high-speed rotors, areas with high static stresses can cause a starting fatigue process. For this reason, the rotor's component strength is studied. Using the Basquin equation, the *S-N* (Wöhler) curve of the studied materials for cyclic load can be estimated [12]:

$$\sigma_A = \sigma_f'(2N)^b, \quad (4)$$

where σ_a is the maximum stress amplitude, N the number of cycles, σ'_f the fatigue coefficient and b the fatigue exponent.

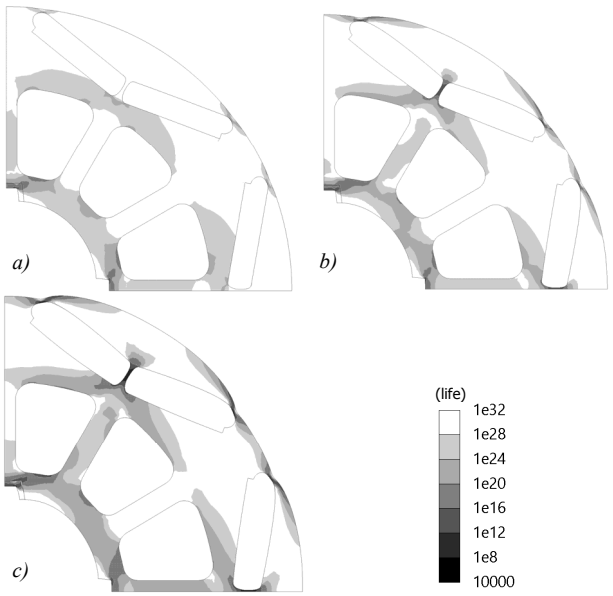

Fig. 3. Simulated life of rotor at 12,000 min^{-1} for M350-50A: *a)* glued magnets, *b)* without magnets, *c)* unglued magnets (magnification scale: 1:170).

For this study, only a cyclic tensile load is applied, so for the stress ratio R follows:

$$R = \frac{\sigma_{\min}}{\sigma_{\max}} \geq 0. \tag{5}$$

$\sigma_{\min}$ is the minimum of cyclic stress whereas $\sigma_{\max}$ is the maximum of cyclic stress. Using the mean stress correction [15], the Wöhler curve is estimated for $R \geq 0$.

In Fig. 3, the results of fatigue simulation for the maximum speed defined by the used electrical machine ($n_{\max}$ = 12,000 min^{-1}) are shown. As expected, the lowest number of cycles until failure (life) appears in the regions with highest mechanical stress (areas around notches at inner rotor radius and magnets fillets). For the configuration with unglued magnets, the minimum number of cycles is about 60,000. However, the estimated life of most rotor areas is beyond the endurance fatigue limit (10^6 cycles).

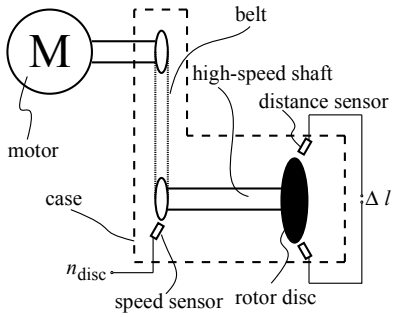

Fig. 4. Measurement setup.

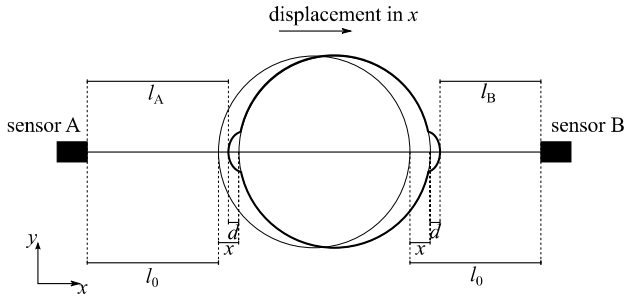

Fig. 5. Laser sensors and corresponding distances.

Before a material which is loaded by cyclic stress reaches its number of cycles to failure, the fatigue process starts with local plastic deformations and microcracks inside the material [16]. This material deterioration before material failure occurs has an influence on the magnetic properties [13]. For this reason, the progress of the material fatigue has to be estimated.

III. Measurement Setup

A. Test Bench Components

The stress distribution inside the rotor lamination causes a corresponding rotor deformation which is mostly dependent on the rotor topology, mechanical properties of the steel grade and speed. Mechanical simulations provide a first estimation of the stress distribution and resulting deformation contour but do not consider any influences due to machine production or cyclic loads. To determine the rotor deformation, a test bench is constructed. This test bench allows an in-situ measurement of the rotor deformation for speeds up to 20,000 min^{-1}.

The test bench consists of an electric drive which is connected to the high-speed shaft by a belt (Fig. 4). Combined with a spindle ball bearing, this configuration ensures a shaft with reduced vibrations. The rotor disc specimens are attached to the high-speed shaft. Two high-resolution laser sensors, placed in opposite to each other, measure the distance to the rotor edge by using laser triangulation. The lasers have a maximum resolution of 40 µs corresponding to an angle resolution of 4.8 ° at 20,000 min^{-1}. The drive and measurement signals (speed, distance) are controlled and visualized by a self-programmed GUI.

B. Rotor Specimens

For this study, a PMSM rotor topology with v-shaped permanent magnets is chosen. Different steel grades are measured to obtain contrastable results. In Tab. 1, the used steel grades with their characteristic mechanical properties are shown.

Different magnet arrangements allow a worst-case and best-case estimation of the stress distribution, knowing that unglued magnets in the pockets cause the highest mechanical stress inside the rotor, whereas glued magnets lead to the lowest mechanical stress distribution (Fig. 1).

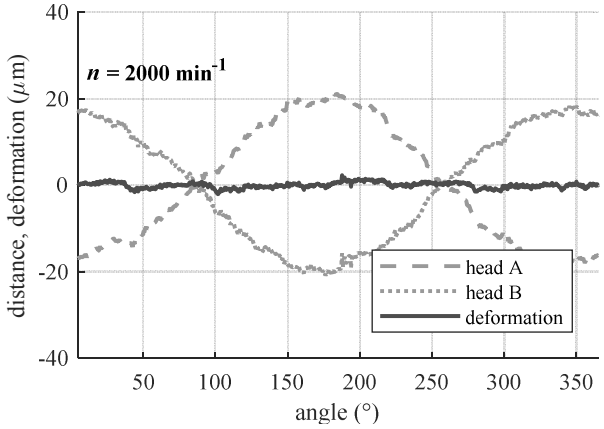

Fig. 6. Measured distance and resulting deformation for M350-50A, without magnets at 2,000 min^{-1}.

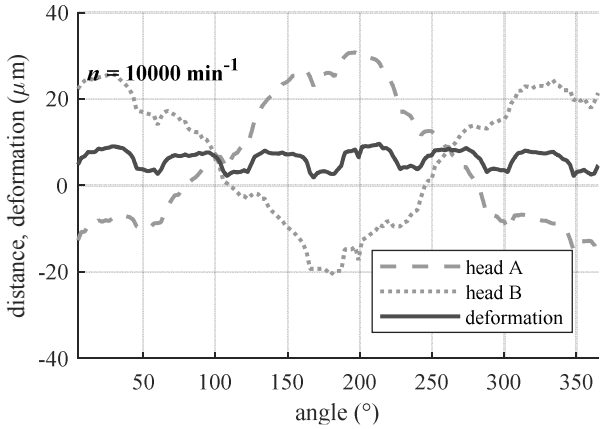

Fig. 7. Measured distance and resulting deformation for M350-50A, without magnets at 10,000 min^{-1}.

C. Determination of rotor deformation

The rotor deformation can be calculated by using the distance measurement results at each position. Knowing that the laser sensors are placed opposite to each other and assuming the rotor deformation d is symmetric, the deformation can be calculated (Fig. 5):

$$\begin{aligned} l_{\mathrm{A}} &= l_0 + x - d, \\ l_{\mathrm{B}} &= l_0 - x - d, \end{aligned} \tag{6}$$

$$\Rightarrow d = l_0 - \frac{1}{2}\left(l_{\mathrm{A}} + l_{\mathrm{B}}\right), \tag{7}$$

where l_{A} and l_{B} are the measured distances of the laser sensors and x a displacement in x-direction. Due to an identical distance of both sensors at starting position, l_0 is set to 0.

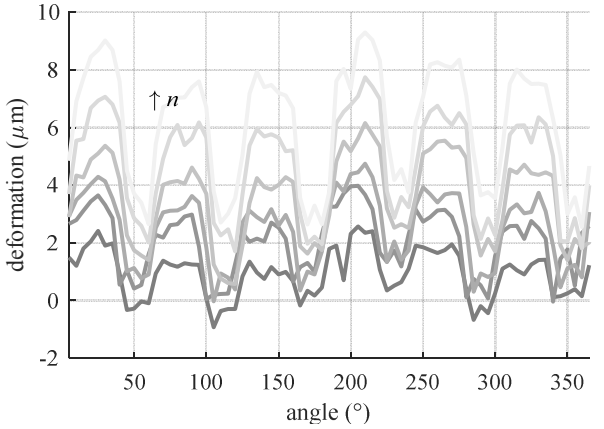

Fig. 8. Resulting deformation contour for M350-50A, cut by fibre-laser and without magnets from 5000 min^{-1} (▬) to 10000 min^{-1} (▬).

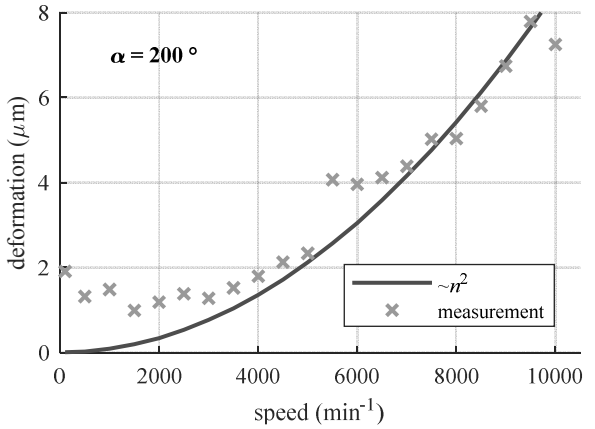

Fig. 9. Speed-dependent deformation for M350-50A, cut by fibre-laser and without magnets at one single rotor position.

IV. Measurement Results

A. Material-dependent deformation

In Fig. 6 and Fig. 7, the measured distances of the laser sensors and the resulting deformation dependent on the rotor position are shown for 2,000 min^{-1} and 10,000 min^{-1}. The distances are superposed by a sinusoidal signal which is caused by a displacement of the shaft. The resulting deformation is not significant for 2,000 min^{-1}. However, a characteristic deformation can be observed for 10,000 min^{-1}. The local maxima are situated at the location of the magnet pockets, whereas the minima are located between the magnet pockets. Regarding the local minima, it can be concluded that the whole rotor is widened at higher speeds.

Fig. 8 depicts the resulting deformation dependent on the rotor speed. The position of the local minima and maxima does not change. However, the deformation is dependent with n^2 and becomes significant for high speeds (Fig. 9).

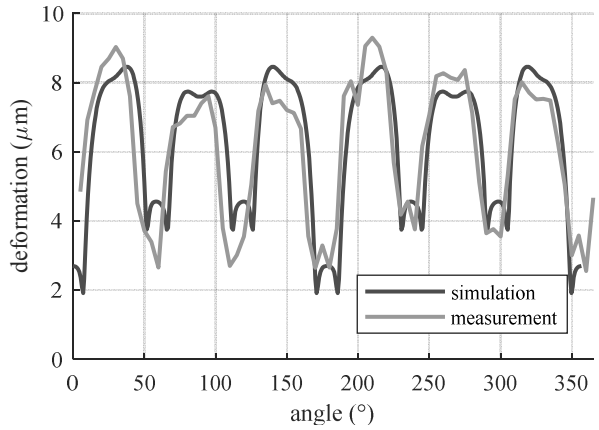

Fig. 10. Comparison of simulation and measurement for M350-50A, without magnets at 10,000 min^{-1}.

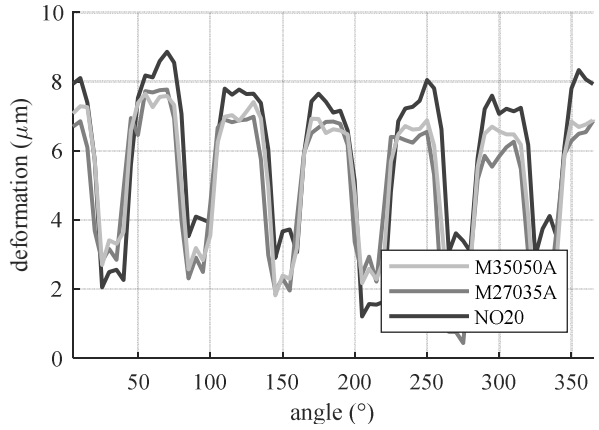

Fig. 11. Deformation for all measured materials, without magnets at 10,000 min^{-1}.

In Fig. 10, the measurement and simulation results are compared. It can be observed that the simulation and measurement are in a good agreement. Due to the centrifugal forces and the geometry of the PMSM rotor, the characteristic minima and maxima are located at the same positions. However, small discrepancies occur caused by measurement uncertainties and a simplified simulation model.

B. Influence of steel grade

The comparison of all measured materials does not show any significant differences between the studied materials (Fig. 11). The characteristic deformation contour with local minima and maxima at the same rotor positions can be observed for all specimens. A greater difference might be observed when using materials with greater differences in the mechanical material properties.

C. Influence of magnet arrangment

The magnet arrangement leads to the expected deformation contours (Fig. 12) when compared to the simulation results (Fig. 2).

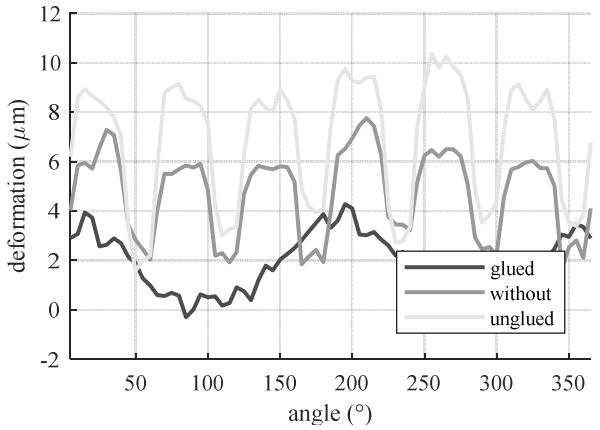

Fig. 12. Deformation dependent on magnet arrangement for M350-50A at 9,000 min^{-1}.

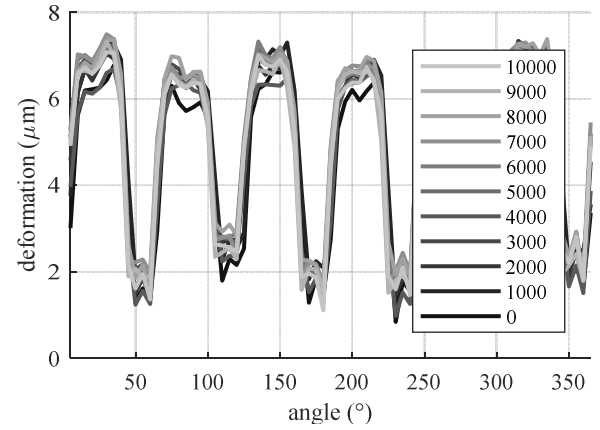

Fig. 13. Deformation dependent on number of cycles for M350-50A at 10,000 min^{-1}.

In this case, the contour for 9,000 min^{-1} is shown because of safety reasons: The maximum speed for the rotor configuration with unglued magnets is limited to this speed. Higher speeds for this configuration cause plastic deformations inside the stack lamination. The measurement result for the rotor configuration with glued magnets does not show any relevant deformation but only an oscillating signal.

D. Cyclic Load

To determine the influence of pulsating stress, one specimen is loaded by a sinusoidal speed:

$$n(t) = \hat{n}\sin(2\pi f t) + \bar{n}, \tag{8}$$

where $\hat{n} = 5,000\,\mathrm{min}^{-1}$, $f = 0.1\,\mathrm{Hz}$ and $\bar{n} = 5,000\,\mathrm{min}^{-1}$. Every 500 cycles, the static deformation for 10,000 min^{-1} is measured, resulting in the characteristic deformation curve. In this study, the maximum number of cycles is set to 10,000.

Fig. 13 depicts the deformation dependent on number of cycles at 10,000 min^{-1}. It can be observed that an influence of a beginning fatigue process is not present and not visible for this maximum number of cycles. All measured deformation characteristics show similar numbers.

V. Conclusions

Rotors of electrical high-speed machines are subject to high centrifugal forces causing high mechanical stresses inside the steel package. In addition, a cyclic mechanical load leads to a beginning fatigue process. Due to the magneto-mechanical effect, the magnetic properties of the steel sheets are altered by these mechanical loads. Thus, it is essential to know the exact mechanical stress distribution inside the rotor.

For this study, a test bench is constructed to perform in-situ measurements of the rotor deformation of PMSM rotors at high speeds. The rotor deformation allows a conclusion to the stress distribution inside the rotor steel package. The used measurement approach with two laser sensors placed opposite to each other enables a distance measurement with a high resolution. It was shown that this deformation contour for high speed corresponds to a particular stress distribution inside the rotor lamination. Furthermore, steel grades and magnet arrangements influence the deformation contour and therefore the stress distribution inside the rotor lamination. The effect of cyclic stresses on the deformation contour could not be observed due to a low number of cycles.

In further studies, the maximum number of cycles will be increased so an influence of the fatigue process will become relevant. In addition, the focus will be shifted to the areas with high mechanical stress, i.e. the fillets around the magnets pockets and the consequences of the shaft-hub joint on the stress distribution.

Acknowledgment

This work is originated as part of the research training group GRK 1856 by the Deutsche Forschungsgesellschaft (DFG).

References

[1] A. Borisavljevic, H. Polinder, and J. A. Ferreira, "On the Speed Limits of Permanent-Magnet Machines," *IEEE Transactions on Industrial Electronics*, vol. 57, no. 1, pp. 220–227, 2010.

[2] S. Elfgen, S. Steentjes, S. Böhmer, D. Franck, and K. Hameyer, "Influences of Material Degradation Due to Laser Cutting on the Operating Behavior of PMSM Using a Continuous Local Material Model," *IEEE Transactions on Industry Applications*, vol. 53, no. 3, pp. 1978–1984, 2017.

[3] B. Riemer, M. Leßmann, and K. Hameyer, "Rotor design of a high-speed Permanent Magnet Synchronous Machine rating 100,000 rpm at 10kW," in *2010 IEEE Energy Conversion Congress and Exposition (ECCE)*, 2010, pp. 3978–3985.

[4] R. M. Bozorth, *Ferromagnetism*. Piscataway, NJ, Hoboken, NJ: IEEE Press; Wiley-Interscience, 1993.

[5] O. Perevertov, J. Thielsch, and R. Schäfer, "Effect of applied tensile stress on the hysteresis curve and magnetic domain structure of grain-oriented transverse Fe-3%Si steel," *Journal of Magnetism and Magnetic Materials*, vol. 385, pp. 358–367, 2015.

[6] N. Leuning, S. Steentjes, M. Schulte, W. Bleck, and K. Hameyer, "Effect of elastic and plastic tensile mechanical loading on the magnetic properties of NGO electrical steel," *Journal of Magnetism and Magnetic Materials*, vol. 417, pp. 42–48, 2016.

[7] A. Belahcen, K. Fonteyn, R. Kouhia, P. Rasilo, and A. Arkkio, "Magnetomechanical coupled FE simulations of rotating electrical machines," *COMPEL - The international journal for computation and mathematics in electrical and electronic engineering*, vol. 32, no. 5, pp. 1484–1499, 2013.

[8] K. Yamazaki and W. Fukushima, "Loss Analysis of Induction Motors by Considering Shrink Fitting of Stator Housings," *IEEE Transactions on Magnetics*, vol. 51, no. 3, pp. 1–4, 2015.

[9] D. Vanoost, S. Steentjes, J. Peuteman, G. Gielen, H. de Gersem, D. Pissoort, and K. Hameyer, "Magnetic hysteresis at the domain scale of a multi-scale material model for magneto-elastic behaviour," *Journal of Magnetism and Magnetic Materials*, vol. 414, pp. 168–179, 2016.

[10] U. Aydin, P. Rasilo, F. Martin, D. Singh, L. Daniel, A. Belahcen, M. Rekik, O. Hubert, R. Kouhia, and A. Arkkio, "Magneto-mechanical modeling of electrical steel sheets," *Journal of Magnetism and Magnetic Materials*, vol. 439, pp. 82–90, 2017.

[11] J. Karthaus, S. Steentjes, N. Leuning, and K. Hameyer, "Effect of mechanical stress on different iron loss components up to high frequencies and magnetic flux densities," *COMPEL - The international journal for computation and mathematics in electrical and electronic engineering*, vol. 36, no. 3, pp. 580–592, 2017.

[12] Y. Gao, R. Long, Y. Pang, and M. Lindenmo, "Fatigue Properties of an Electrical Steel and Design of EV/HEV IPM Motor Rotors for Durability and Efficiency," *SAE Technical Paper 2010-01-1308*, 2010.

[13] J. Karthaus, S. Steentjes, D. Gröbel, K. Andreas, M. Merklein, and K. Hameyer, "Influence of the mechanical fatigue progress on the magnetic properties of electrical steel sheets," *Archives of Electrical Engineering*, vol. 66, no. 2, pp. 351–360, 2017.

[14] M. K. Devine, D. C. Jiles, and S. Hariharan, "Effects of cyclic stress on the magnetic hysteresis parameters of polycrystalline iron," *Journal of Magnetism and Magnetic Materials*, vol. 104-107, pp. 377–378, 1992.

[15] C. Berger, *Fracture mechanics proof of strength for engineering components,* 3rd ed. Frankfurt am Main: VDMA, 2009.

[16] Y. Murakami, S. Kodama, and S. Konuma, "Quantitative evaluation of effects of non-metallic inclusions on fatigue strength of high strength steels. I: Basic fatigue mechanism and evaluation of correlation between the fatigue fracture stress and the size and location of non-metallic inclusions," *International Journal of Fatigue*, vol. 11, no. 5, pp. 291–298, 1989.